© 2015. Published by The Company of Biologists Ltd | Development (2015) 142, 375-384 doi:10.1242/dev.112680

RESEARCH ARTICLE

Calm1 signaling pathway is essential for the migration of mouse precerebellar neurons

Hiroaki Kobayashi‡, Shunsuke Saragai, Atsushi Naito, Koji Ichio, Daisuke Kawauchi* and Fujio Murakami

ABSTRACT

The calcium ion regulates many aspects of neuronal migration, which is an indispensable process in the development of the nervous system. Calmodulin (CaM) is a multifunctional calcium ion sensor that transduces much of the signal. To better understand the role of Ca^{2+}-CaM in neuronal migration, we investigated mouse precerebellar neurons (PCNs), which undergo stereotyped, long-distance migration to reach their final position in the developing hindbrain. In mammals, CaM is encoded by three non-allelic CaM (Calm) genes (*Calm1*, *Calm2* and *Calm3*), which produce an identical protein with no amino acid substitutions. We found that these CaM genes are expressed in migrating PCNs. When the expression of CaM from this multigene family was inhibited by RNAi-mediated acute knockdown, inhibition of *Calm1* but not the other two genes caused defective PCN migration. Many PCNs treated with *Calm1* shRNA failed to complete their circumferential tangential migration and thus failed to reach their prospective target position. Those that did reach the target position failed to invade the depth of the hindbrain through the required radial migration. Overall, our results suggest the participation of CaM in both the tangential and radial migration of PCNs.

KEY WORDS: Precerebellar neuron, Migration, *Calm1*, Calcium signaling, Pontine nuclei

INTRODUCTION

The calcium ion is a remarkably simple and versatile second messenger that mediates a wide spectrum of cellular functions. Calmodulin (CaM) is a multifunctional calcium ion sensor protein that transduces much of the calcium signaling. CaM is a dumbbell-shaped molecule in which two structurally similar globular domains, each containing a pair of EF-hand calcium-binding motifs, are separated by a long flexible central helix (Ikura and Ames, 2006). This structure allows conformational plasticity in CaM and its binding to a large number and diverse array of downstream target proteins (Berggård et al., 2006; Ikura and Ames, 2006). Interestingly, CaM is evolutionarily highly conserved and exists in identical form with no amino acid substitutions in all vertebrates, suggesting both a rigid requirement for its structure and its indispensability for calcium signaling (Friedberg and Rhoads, 2001).

In the developing nervous system, one important function of calcium signaling is the regulation of neuronal motility. Newly born neurons undergo a directed migration from their birthplace to the appropriate target position, which is an indispensable process for the subsequent wiring of the neural circuit (Hatten, 2002; Ayala et al., 2007; Marín et al., 2012). Calcium signaling has been implicated in many aspects of this migration, including nucleokinesis and directional navigation (Zheng and Poo, 2007). To further elucidate the role of calcium signaling, we studied the involvement of CaM in neuronal migration.

We focused on the migration of hindbrain precerebellar neurons (PCNs). PCN migration is a suitable model owing to its long, highly confined stereotyped migratory path and the genetic tractability of this path (Kawauchi et al., 2006; Okada et al., 2007). PCNs refer to neurons constituting a collection of discrete medullary and pontine nuclei that provides input to the cerebellum (Altman and Bayer, 1987a,b, 1997). These neurons originate from the dorsal margin of the hindbrain, known as the lower rhombic lip (LRL), and diverge into three discrete tangential migratory streams: the anterior extramural stream (AEMS), which gives rise to the pontine nucleus (PN) in the pons; the posterior extramural stream (PEMS), which gives rise to the external cuneate nucleus (ECN) and the lateral reticular nucleus (LRN) in the medulla; and the intramural circumferential pathway, which gives rise to the inferior olivary nucleus (ION) in the medulla. After reaching the appropriate circumferential position via tangential migration, PCNs comprising the AEMS and PEMS then invade into the depth of the hindbrain to form nuclei by radial migration along radial glial fibers (Kawauchi et al., 2006). Therefore, this system allows us to study both tangential and radial modes of migration.

To genetically manipulate CaM function in PCNs, we utilized an RNAi-mediated acute knockdown approach. Intriguingly, in mammals CaM is encoded by a family of three non-allelic genes (*Calm1*, *Calm2* and *Calm3*) that produce an identical protein with no amino acid substitutions (Toutenhoofd and Strehler, 2000). It is hypothesized that these three CaM transcripts provide distinct local pools of CaM protein through post-transcriptional regulation to meet various demands for its cellular functions (Toutenhoofd and Strehler, 2000; Palfi et al., 2002). On the basis of this genomic organization, we conducted RNAi-mediated acute knockdown of each of the three CaM genes.

Here, we show that all three CaM genes are expressed in migrating PCNs. Using shRNAs specific to each member of the CaM gene family, we demonstrated that *Calm1* plays a dominant and crucial role in PCN migration. Many PCNs treated with *Calm1* shRNA failed to reach the appropriate circumferential position by E17.5 and were still located in the migratory pathway. Those that reached the prospective target region did not invade the depth of the prospective nucleus through the required radial migration and were confined superficially. These results uncovered an essential role of *Calm1* in tangential migration and possibly also in radial migration along the radial glia.

RESULTS

Expression of all three CaM genes in migrating PCNs

We first examined which of the three CaM genes are expressed by migrating PCNs (Fig. 1). PCNs were identified by *in situ*

Graduate School of Frontier Biosciences, Osaka University, Suita, Osaka 565-0871, Japan.
*Present address: German Cancer Research Center, Heidelberg 69120, Germany.

‡Author for correspondence (hirokob@fbs.osaka-u.ac.jp)

Received 13 May 2014; Accepted 21 November 2014

Development (2015) 142, 375-384 doi:10.1242/dev.112680

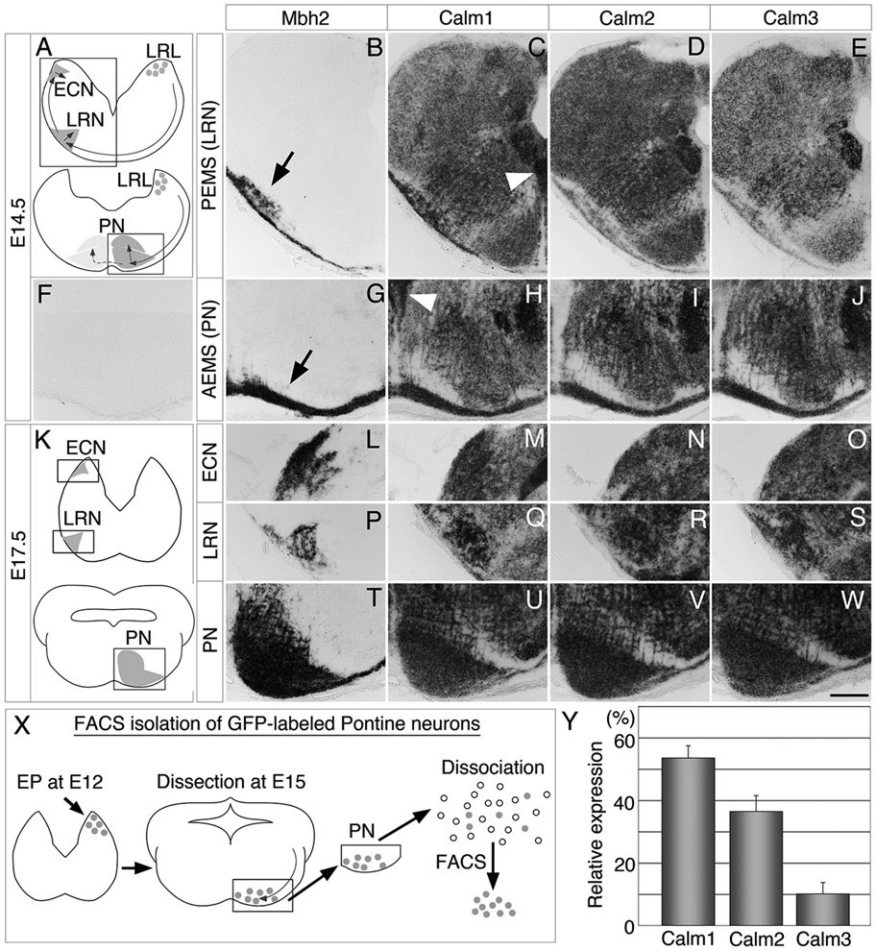

Fig. 1. Expression of CaM mRNAs in the AEMS and PEMS of the developing mouse hindbrain. (A) Schematic representation of the two migratory pathways of PCNs. While LRN/ECN neurons cross the midline and form nuclei on the contralateral side to their originating LRL, most PN neurons settle on the ipsilateral side with a small population contributing to the contralateral nucleus. Boxed regions indicate the visual fields shown in B-E (top box) and F-J (bottom box). Adjacent sections at the level of the AEMS and PEMS of mouse hindbrains at E14.5 (B-J) or E17.5 (L-W) were subjected to *in situ* hybridization (ISH) for *Mbh2*, *Calm1*, *Calm2* or *Calm3*. (F) AEMS hybridized with control sense RNA probes for *Calm1*. (K) Schematic representations showing the position of the imaged areas in L-O (top box), P-S (middle box) and T-W (bottom box). Arrows indicate LRN neurons in the PEMS that have crossed the midline and reached the contralateral prospective LRN region (B), while PN neurons have just reached the ipsilateral prospective PN region (G). Only *Calm1* was expressed in the floor plate (arrowheads in C,H). AEMS, anterior extramural stream; PEMS, posterior extramural stream; LRL, lower rhombic lip; PN, pontine nucleus; ECN, external cuneate nucleus; LRN, lateral reticular nucleus. Scale bar: 200 µm. (X) Scheme of FACS isolation of GFP-labeled PN neurons. The LRL was electroporated with GFP-expressing plasmids at E12.5, and the ventral tissue containing fluorescent PN neurons was dissected. GFP-labeled PN neurons were then dissociated and sorted by FACS. (Y) Relative copy numbers of the three CaM transcripts expressed in PN neurons (mean±s.d.). The amount of each CaM transcript in the cDNAs generated from the FACS-sorted PN neurons was measured by real-time quantitative PCR. *n*=10 measurements from three independent cDNAs, each of which was derived from 8-9 embryos.

hybridization (ISH) with the marker *Mbh2* (also known as *Barhl1*) (Bulfone et al., 2000; Li et al., 2004; Kawauchi et al., 2006). Transcripts from the three CaM genes were distinguished by cRNA probes of 600-800 nucleotide sequences within their 3′UTR, where no sequence similarities are found.

First, we examined expression at E14.5, when the majority of PCNs are actively migrating. LRN neurons in the PEMS have crossed the midline and reached the contralateral prospective LRN region (Fig. 1B), while PN neurons have just reached the ipsilateral prospective PN region (Fig. 1G) (Watanabe and Murakami, 2009; Shinohara et al., 2013). All three CaM genes were expressed in the migratory pathway of PCNs and in most hindbrain areas, with relatively strong expression in the brainstem motor nuclei (Xth and XIIth motor nuclei). The overall spatial expression of the three CaM genes was similar, with slight differences. For example, only *Calm1* was expressed in the floor plate (FP) (Fig. 1C-E,H-J). *Calm1* expression in the LRN region was relatively high compared with its surroundings, whereas *Calm2* and *Calm3* appeared low (Fig. 1C-E). Expression of all three CaM genes was also detected in the AEMS (Fig. 1H-J). We also examined expression at E17.5, when the majority of PCNs have settled at their final position (Kawauchi et al., 2006; Shinohara et al., 2013). We found that all three CaM genes were expressed in the ECN (Fig. 1M-O), LRN (Fig. 1Q-S) and PN (Fig. 1U-W).

To directly quantify relative expression, we performed real-time quantitative PCR using PN neuron-specific cDNA. For this purpose, the LRL was electroporated with plasmids expressing GFP at E12.5. In mice, the peak of LRN/ECN neuron generation is around E12, that of PN neurons is around E12-14, and that of ION neurons is earlier at around E10 (Taber Pierce, 1966, 1973; Kawauchi et al., 2006; Shinohara et al., 2013). Therefore, electroporation at E12.5 can simultaneously label PN and LRN/ECN neurons, but avoids labeling ION neurons. The resulting fluorescent PN neurons were dissected and FACS sorted at E15.5 (Fig. 1X). cDNA was generated and the relative abundance of the three CaM transcripts was measured. As shown in Fig. 1Y, *Calm1* comprised 53.5±4.0% of total CaM mRNAs, with *Calm2* and *Calm3* at 36.4±5.1% and 10.1±3.6%, respectively. This result confirmed that all three CaM genes are expressed in PN neurons, with the major contribution from *Calm1*.

To examine the differential expression of the three CaM genes at single-neuron level, we performed ISH on singly cultured PCNs. The LRL explant from E12.5 hindbrain was cultured on a coverslip coated with Matrigel. After 3 days in culture, motile cells having a long leading process emigrated from the explants (Fig. 2A). In total, 74.8% of DAPI-stained cells (113/151 cells) located outside the explants were MAP2-positive neurons (Fig. 2A). Among these, 99.1% (112/113 neurons) were *Mbh2* positive and hence were identified as PCNs (Fig. 2A,B). Therefore, in the following experiments, we used MAP2 immunostaining to identify cultured PCNs. In these MAP2-positive PCNs, all three CaM genes were expressed at a similar subcellular location, mostly in the proximal region of the leading process and the trailing process (Fig. 2C-E). *Calm1*, *Calm2* and *Calm3* were expressed in 88% (73/83 cells), 83% (81/98 cells) and 92% (94/102 cells) of MAP2-positive PCNs, respectively. This result suggested that a single PCN expresses multiple CaM transcripts.

Development (2015) 142, 375-384 doi:10.1242/dev.112680

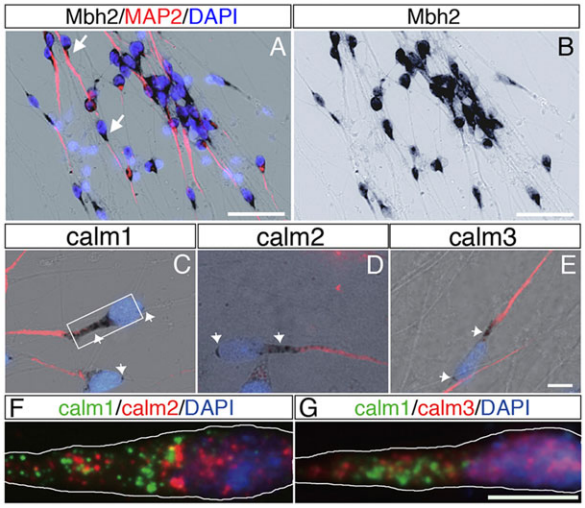

Fig. 2. Distribution of CaM mRNAs in cultured PCNs. (A) Bright-field photomicrograph of cultured PCNs stained by ISH for *Mbh2* (dark purple, arrows) and merged with fluorescence signals for anti-MAP2 immunostaining (red) and nuclear staining with DAPI (blue). (B) Bright-field image of A showing only the ISH. (C-E) Bright-field photomicrographs stained by ISH for each CaM gene member and merged with anti-MAP2 immunostaining and nuclear staining with DAPI. All three CaM genes are expressed at a similar subcellular location in PCNs, mostly in the proximal region of the leading process and the trailing process (arrows). The boxed region in C is magnified in F,G. (F,G) Dual-fluorescence ISH for co-expression of CaM genes. Merged images of the FITC and Cy3 signals indicating a pair of CaM genes, as indicated at the top, overlaid with DAPI signal. The proximal regions of the leading processes are shown (outlined). Scale bars: 50 µm in A,B; 20 µm in C-E; 10 µm in F,G.

By performing fluorescent *in situ* hybridization (FISH), we directly examined the simultaneous expression of a pair of CaM gene family members and their subcellular localization at higher spatial resolution. Fig. 2F shows an example of the proximal region of the leading process probed for *Calm1* and *Calm2*. This PCN clearly expressed both *Calm1* and *Calm2* transcripts, although the signals rarely overlapped (Fig. 2F). All PCNs examined for the expression of *Calm1* and *Calm2* expressed both transcripts (n=88 cells), as was also the case for *Calm1* and *Calm3* (Fig. 2G; n=35 cells). From these results, we concluded that each PCN expresses all three CaM genes simultaneously, although the localization of each CaM transcript differs.

Gene-specific knockdown of CaM gene family members by shRNA

To reveal the role of the CaM genes in PCN migration, we generated a series of plasmids that produce shRNAs that specifically target each gene. When expressed in COS7 cells along with a YFP-tagged CaM reporter, each shRNA suppressed the expression of the reporter carrying its target CaM gene but not that of reporters carrying non-target CaM genes (Fig. 3A). For example, *Calm1*sh361, which targets *Calm1* mRNA, suppressed the expression of YFP-Calm1 but not that of YFP-Calm2 or YFP-Calm3. The efficiency and the specificity of the knockdown exerted by the three shRNAs are summarized in Fig. 3B. *Calm1*sh361 inhibited the expression of YFP-Calm1 to 7.1±2.5% of the control plasmid, *Calm2*sh414 inhibited YFP-Calm2 to 10.3±1.9%, and *Calm3*sh384 inhibited YFP-Calm3 to 11.8±2.2%.

We then examined the effectiveness of these shRNAs on endogenous CaM mRNAs expressed in migrating PCNs *in vivo*. The LRL was electroporated at E12.5 with plasmids expressing GFP and shRNA, then the GFP-labeled PN neurons were dissected and FACS sorted at E15.5, and cDNA was generated. Real-time quantitative PCR was performed and the percentage CaM gene expression in shRNA-treated PN neurons relative to that in untreated control PN neurons was calculated. Knockdown by *Calm1*sh361 suppressed the expression of endogenous *Calm1* mRNA to 18.9±3.2% of control. Similarly, *Calm2*sh414 and *Calm3*sh384 reduced

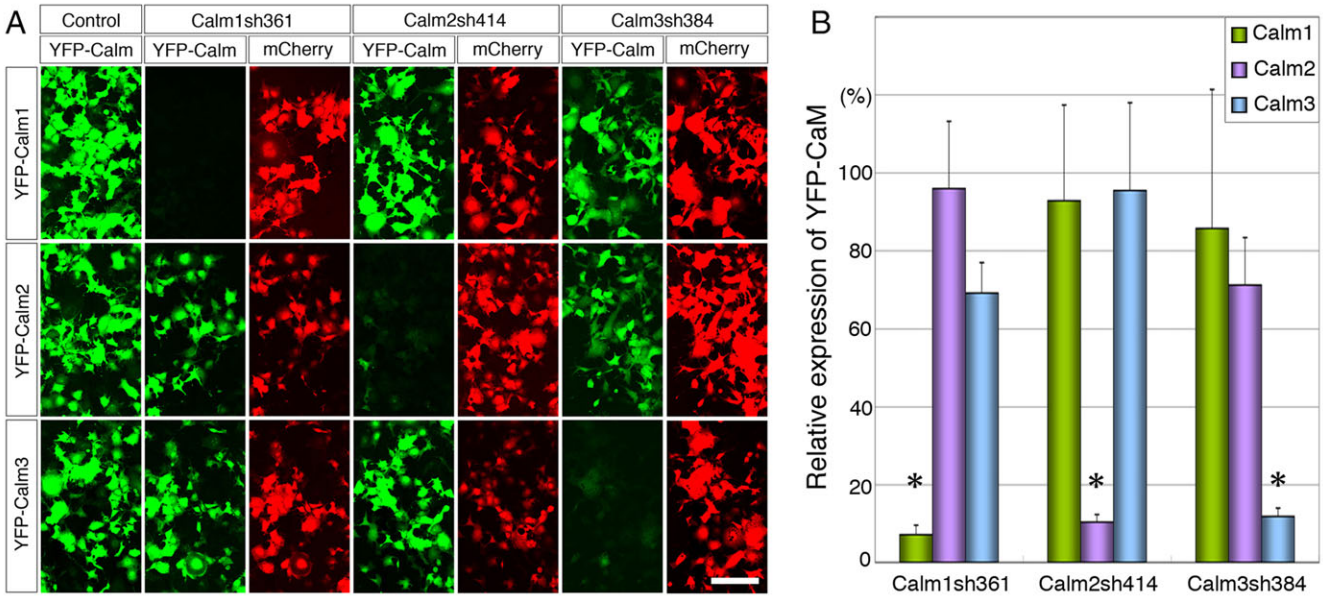

Fig. 3. Gene-specific knockdown by shRNAs targeted to each CaM gene family member. (A) The effect of CaM shRNAs on the expression of exogenously introduced EYFP-tagged CaM. COS7 cells were transfected with plasmids encoding EYFP-tagged CaM (as indicated on the left), plasmids for mCherry and plasmids encoding shRNA (as indicated at the top). For each combination of plasmids, a pair of YFP and mCherry images from the same visual field is shown. Scale bar: 200 µm. (B) Quantification of the effect of shRNAs. Shown is EYFP-CaM expression (normalized value as EYFP over mCherry fluorescence) in shRNA-treated COS7 cells as a percentage of that in control COS7 cells (mean±s.d.). n=4 independent visual fields containing ~100 transfectants from two independent experiments. *P=0.0143, one-tailed Mann–Whitney U-test, shRNA-treated versus control cells.

Development (2015) 142, 375-384 doi:10.1242/dev.112680

the expression of *Calm2* and *Calm3* to 32.1±10.2% and 27.8±5.4%, respectively (n=4 measurements from pooled cDNAs, each derived from of 8-21 embryos). Persistent reduction of endogenous *Calm1* expression by *Calm1*sh361 was observed at E17.5 by ISH (data not shown).

Calm1 is essential for the migration of PCNs

We then examined the effect of the shRNAs on the migration of PCNs. We electroporated plasmids expressing GFP and shRNAs into PCNs residing in the LRL of E12.5 mouse embryos. The embryos were analyzed at E17.5, when the majority of PCNs had arrived at their target regions (Kawauchi et al., 2006; Okada et al., 2007; Kobayashi et al., 2013; Shinohara et al., 2013). Fig. 4 shows a ventral view of whole-mount hindbrain in which the PN and the LRN are discernible. The majority of PCNs treated with control shRNA had arrived at the target region by E17.5, and few neurons remained in the migrating paths (Fig. 4B,C; n=6). By contrast, a substantial number of *Calm1*sh361-treated PCNs failed to reach their targets, remaining in the path to the PN (Fig. 4D, arrowhead; n=7/7) or LRN (Fig. 4E, arrowhead) and between the LRN and ECN (Fig. 4E, arrow). Similar tangential migration defects were observed with another shRNA targeted to the *Calm1* gene, *Calm1*sh427. The defect caused by *Calm1*sh427 was even more severe than that of *Calm1*sh361, as fewer PN neurons reached the prospective PN region, while more PN neurons lingered in the migratory pathway (Fig. 4F, arrowhead). In the PEMS, many LRN/ECN neurons were stuck at the midline, failing to cross it (Fig. 4G, arrow). This defect in tangential migration was not observed with *Calm2*sh414 (n=0/6) or with *Calm3*sh384 (n=0/13) (Fig. 4H-K).

PCNs first arrive at the prospective target region by tangential migration, then migrate radially along the radial glial fibers, and finally invade into and populate the depth of the nucleus (Kawauchi et al., 2006; Watanabe and Murakami, 2009; Shinohara et al., 2013). To analyze this radial migration, transverse sections of the PN were examined at E17.5 (Fig. 5). Normally by this stage, many PN neurons have entered and populated the dorsal region of the nucleus, forming the outline of the mature PN, although they were still motile, adjusting their final position within the nucleus (Fig. 5A, control shRNA) (Shinohara et al., 2013). In clear contrast, most *Calm1*sh361-treated PN neurons failed to migrate into the dorsal PN. Instead, they tended to remain superficial and accumulated in the ventral PN (Fig. 5A). Furthermore, *Calm1*sh361-treated PN neurons also accumulated at the midline, which was rarely observed in the control at this stage (Fig. 5A). In accordance with the tangential migration defect observed in whole-mount preparations, this failure of radial migration within the PN was *Calm1*sh361 specific, as it was rarely seen in *Calm2*sh414- or *Calm3*sh384-treated PN neurons (Fig. 5A).

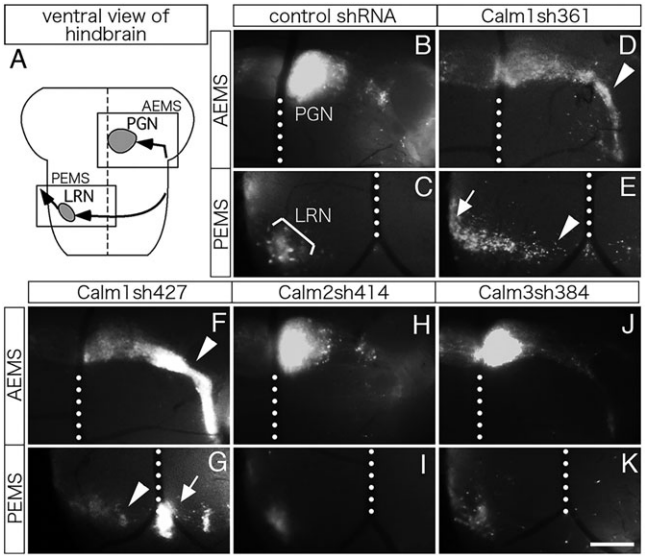

Fig. 4. Tangential migration defects of PCNs caused by *Calm1* shRNA. PCNs were co-transfected with GFP-expressing and shRNA-expressing plasmids at E12.5 and examined at E17.5. (A) Schematic ventral view of a whole-mount hindbrain. Anterior is up. Arrows indicate the two migratory pathways of PCNs. Boxed regions indicate the AEMS and PEMS regions shown in B,D,F,H,J and C,E,G,I,K, respectively. (B-K) Fluorescence photomicrographs of the whole-mount hindbrain showing the distribution of GFP-labeled PCNs treated with control shRNA (B,C), *Calm1*sh361 (D,E), *Calm1*sh427 (F,G), *Calm2*sh414 (H,I) or *Calm3*sh384 (J,K). Dotted lines indicate the midline. Arrowheads and arrows indicate aberrantly positioned PCNs. Scale bar: 500 µm.

To analyze the extent of radial migration among shRNA-treated PN neurons, we quantified the ratio of the area occupied by fluorescently labeled neurons that had entered the dorsal PN to that in the entire nucleus (Fig. 5B,C). Whereas 36.2±11.4% of control PN neurons were distributed in the dorsal region, only 8.6±5.1% of *Calm1*sh361-treated PN neurons did (Fig. 5C; Mann–Whitney U-test, P=0.0004). *Calm1*sh427 caused similar defects, with 17.3±3.8% of *Calm1*sh427-treated PN neurons found in the dorsal region (Fig. 5C; Mann–Whitney U-test, P=0.0007). However, for *Calm2*sh414-, *Calm2*sh285-, *Calm3*sh384- and *Calm3*sh408-treated PN neurons, 34.5±4.5%, 41.5±5.0%, 37.5±12.8% and 46.7±16.1% reached the dorsal region, respectively – results not statistically different from the control (Fig. 5C). The substantial accumulation of *Calm1*-deficient PN neurons in the migratory path to the PN observed in whole-mount specimens (Fig. 4D,F) was also evident in transverse sections. We calculated the ratio of the area occupied by fluorescent cells in the path to that observed in the entire section (Fig. 5D,E). Whereas only 7.5±4.8% of control PN neurons were found in the path, 22.7±9.8% of *Calm1*sh361-treated PN neurons remained there (Fig. 5E; Mann–Whitney U-test, P=0.0067).

Based on the findings of *Calm1* participation in PCN migration, we then examined the temporal profile of the migration defects caused by *Calm1*sh361 in more detail. We first examined the migration of PCNs at E15.5. There was no discernible difference between control and *Calm1*sh361-treated PCNs when PCN distribution in the hindbrain was examined in whole-mount configurations. In both the control and *Calm1*sh361 treatment, the leading PEMS population had similarly crossed the midline and entered the contralateral side, and the leading AEMS population had similarly reached the prospective PN regions at the ventral midline (data not shown). Upon examining transverse sections of the hindbrain, the first indications of migration defects were seen. In control preparations, the leading AEMS population that had reached the midline started to invade the prospective PN region along radial glial fibers (Fig. 6A,B). By contrast, only a few *Calm1*sh361-treated PN neurons associated with these fibers (Fig. 6D,E). Similarly, whereas the control PEMS population at the prospective LRN region frequently associated with radial glial fibers, *Calm1*sh361-treated PCNs did so rarely (Fig. 6C,F). We quantified the ratio of PN neurons that were engaged in radial migration at E15.5. Since radially migrating PN neurons were easily distinguishable from tangentially oriented neuronal mass at E15.5, we divided these two populations at the sharp dorsal border of the tangentially migrating mass (Fig. 6G) and calculated the ratio of PN neurons in the radially migrating area (Fig. 6H). Whereas 24.0±11.8% of control PN neurons were engaged in radial migration, only 4.2±2.5% of

Development (2015) 142, 375-384 doi:10.1242/dev.112680

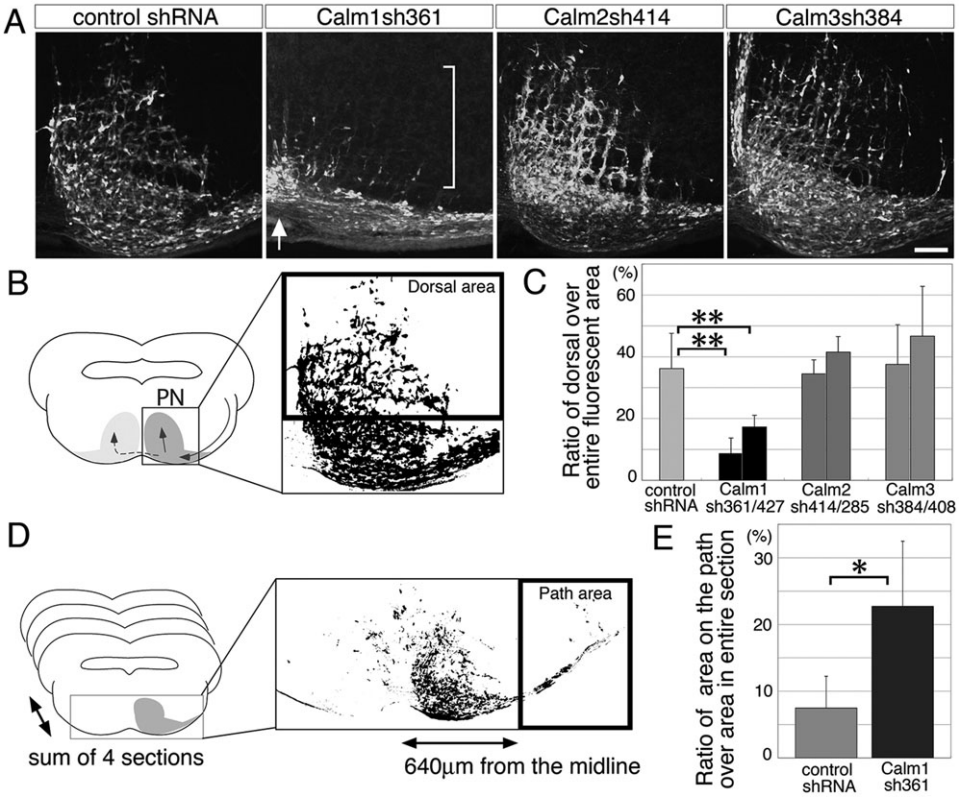

Fig. 5. Radial migration defects of PN neurons caused by *Calm1* shRNAs. PCNs were co-transfected with GFP-expressing and shRNA-expressing plasmids at E12.5 and examined at E17.5. (A) The distribution of GFP-labeled PN neurons in transverse sections of the PN. Arrow indicates the accumulation of *Calm1*sh361-treated PN neurons at the midline. Bracket indicates the area that control PCNs normally populate. The area imaged is boxed in B, with the midline to the left and the pial surface to the bottom. Scale bar: 100 μm. (B) Scheme employed in quantification of the dorsoventral distributions of PN neurons. The ratio of fluorescent area in the dorsal two-thirds of the frame over that in the entire frame was calculated as an index of radial migration (see Materials and Methods for details). (C) Quantification of dorsally located PN neurons according to the methods explained in B (mean±s.d.). ***P*<0.001, Mann–Whitney *U*-test; *n*=6 brains (18 sections) for control; *n*=9 (26) for *Calm1*sh361; *n*=8 (24) for *Calm1*sh427; *n*=5 (15) for *Calm2*sh414; *n*=5 (15) for *Calm2*sh285; *n*=10 (30) for *Calm3*sh384; *n*=5 (15) for *Calm3*sh408. (D) Scheme employed in quantification of pathway accumulation of PN neurons. The ratio of the fluorescent area located farther than 640 μm from the midline (path area) to that in the entire section was calculated. (E) Quantification of PN neurons in the path according to the method explained in D (mean±s.d.). **P*<0.01, Mann–Whitney *U*-test; *n*=6 brains for control; *n*=6 brains for *Calm1*sh361.

*Calm1*sh361-treated PN neurons were (Fig. 6G; Mann–Whitney *U*-test, *P*=0.0079).

We then visualized the morphology of each PN neuron at E16.5 by a sparse labeling method using the Cre-loxP system (Kanegae et al., 1995; Kobayashi et al., 2013). We did not observe a morphological difference between tangentially migrating PN neurons treated with control shRNA or with *Calm1*sh361. In both cases, PN neurons exhibited bipolar morphology, extending a long leading process toward the midline (Fig. 7B,C, arrowheads). In the control, radially migrating neurons were frequently observed (Fig. 7B, arrows). These neurons oriented a short, thick leading process in the radial direction, sometimes making branches (Fig. 7D-F). In the case of *Calm1*sh361 treatment, radially migrating PN neurons were rarely observed at this labeling density. However, when found in the radially deviated position from the tangentially migrating population (Fig. 7C, arrow), they tended to extend multiple fine processes instead of a single thick leading process (Fig. 7G-I).

We also examined whether there was an increase in cell death at E17.5 caused by the reduced CaM expression. Fragmented DNA in dying cells was detected by anti-single-stranded DNA (ssDNA) antibody. The ssDNA signal was occasionally detected among the GFP-labeled PN neurons treated with control shRNA or *Calm1*sh361 (Fig. 7K-N). We did not observe a pronounced increase in the ssDNA signal caused by *Calm1*sh361. The ssDNA signal was also observed in the contralateral hemisphere of *Calm1*sh361-treated brain where untreated PN neurons resided, suggesting that the signal was independent of shRNAs.

Lastly, we analyzed the distribution of PCNs at E18.5, when the majority of PN neurons are stationary and PN nucleogenesis appears complete (Shinohara et al., 2013), to assess whether the migration defect caused by *Calm1*sh361 is a delay or a halt to migration. PCNs treated with *Calm1*sh361 still remained in the path when examined in whole-mount configuration (Fig. 8E,F, arrowheads). They failed to properly populate the prospective PN or LRN regions. Instead, they remained superficially in their respective nucleus: most PN neurons accumulated in ventral PN (Fig. 8G), while many LRN neurons remained in the tangential migratory pathway (Fig. 8H, arrowheads). We quantified the ratio of dorsally located PN neurons by measuring their occupation area (Fig. 8I). Whereas 49.4±13.7% of control PN neurons were distributed in the dorsal region, only 12.6±5.1% of *Calm1*sh361-treated PN neurons were (Fig. 8I; Mann–Whitney *U*-test, *P*=0.0079). These results suggest that the observed phenotypes are more likely to be caused by a cessation of migration, rather than by a delay to migration.

DISCUSSION

To reveal the role of Ca^{2+}-CaM signaling in migrating PCNs, we examined the tissue and subcellular expression of three CaM

Development (2015) 142, 375-384 doi:10.1242/dev.112680

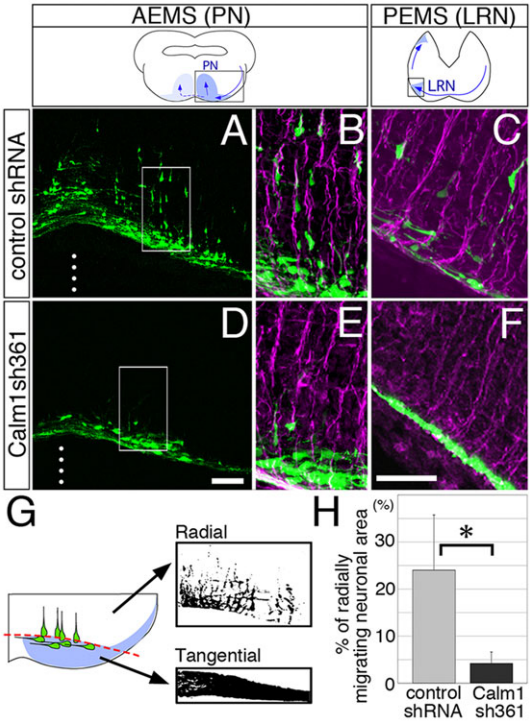

Fig. 6. Effects of *Calm1*sh361 on the migration of PCNs at E15.5. (A-F) PCNs were co-transfected with GFP-expressing and control shRNA-expressing plasmids (A-C) or *Calm1*sh361-expressing plasmids (D-F) at E12.5 and examined at E15.5. Fluorescence photomicrographs of transverse sections of the hindbrain at the level of the PN (A,B,D,E) and the LRN (C,F) as indicated at the top. (B,E) Higher magnification of the boxed areas in A,D. (B,C,E,F) GFP images were overlaid with anti-nestin immunostaining signal (purple) to visualize radial glial fibers. Dotted lines indicate the midline. Scale bars: 80 µm in A,D; 50 µm in C,F. (G) Schematic illustration of the separation of radially migrating neuronal area from tangentially oriented neuronal mass at its dorsal border (red dashed line). (H) The percentage of radially migrating neuronal area among the entire fluorescent area according to the method illustrated in G (mean±s.d.). *P<0.01, Mann–Whitney U-test; n=5 brains (15 sections) for control; n=5 brains (15 sections) for *Calm1*sh361.

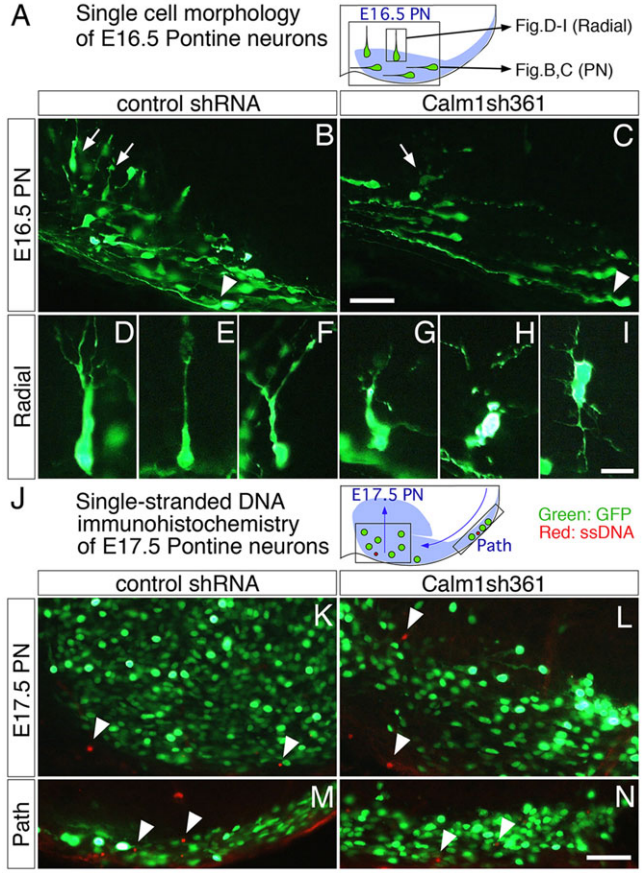

Fig. 7. Morphology of PN neurons and the frequency of cell death. PCNs were co-transfected with GFP-expressing and shRNA-expressing plasmids at E12.5 and examined at E16.5 (A-I) or at E17.5 (J-N). (A-I) Morphology of E16.5 PN neurons treated with control shRNA (B,D-F) or *Calm1*sh361 (C,G-I) as visualized by the sparse labeling method. Arrowheads indicate the long leading processes extended toward the midline by PN neurons in both the control and *Calm1*sh361 conditions. Arrows indicate radially migrating neurons, which were frequently observed in the control (B) but rarely observed with *Calm1*sh361 treatment (C). (A) Schematized view of the PN region showing the positions of the areas imaged in B-I. (B,C) Ventral PN. (D-I) High magnification views of radially oriented PN neurons. (J-N) Anti-ssDNA immunohistochemistry on sections of E17.5 hindbrain treated with control shRNA (K,M) or *Calm1*sh361 (L,N). (J) Schematized view of the hindbrain showing the position of the imaged area for the PN (K,L) and for the pathway (M,N). (K-N) Merged images of GFP signal and ssDNA signal, showing that the ssDNA signal was only occasionally detected among the GFP-labeled PN neurons treated with control shRNA or *Calm1*sh361 (arrowheads). Scale bars: 50 µm in B,C,K-N; 20 µm in D-I.

transcripts in these neurons and found that multiple CaM genes are expressed in the proximal regions of their leading processes and in the trailing processes. RNAi with shRNA targeted to the *Calm1* transcript caused both tangential and radial migration defects, which prevented arrival at the prospective nucleus regions. By contrast, shRNAs targeted to the two other CaM genes did not cause apparent migration defects.

The role of Ca^{2+}-CaM signaling in the migration of PCNs

We have shown that CaM is essential for the proper migration of PCNs. Two types of migration defect were observed: (1) incomplete tangential migration with failure to reach the appropriate circumferential position; and (2) a failure of radial migration to invade the depth of the prospective nucleus regions.

Since CaM can interact with a vast number of downstream proteins (Berggård et al., 2006), it is possible that *Calm1*sh361 inhibits multiple Ca^{2+} signaling cascades simultaneously. We consider possible cellular defects caused by *Calm1*sh361 and the underlying signaling cascades below.

One possible mechanism for the incomplete tangential migration phenotype is a failure to recognize guidance cues at the midline. PCNs treated with *Calm1*sh361 took the correct ventriculo-pial position and migrated abutting the pial meninges. PN neurons migrated anteriorly toward the trigeminal nerve roots, and finally turned medially toward the midline FP, while LRN/ECN neurons took the separate posterior pathway. No PCNs treated with *Calm1*sh361 were observed to deviate from the stereotyped pathway. However, fewer PN neurons migrated medially to reach the prospective PN, and those that reached the midline remained in the FP, a property rarely observed in the control at E17.5. LRN/ECN neurons treated with *Calm1*sh427 also remained at the midline. These observations suggest that the guidance toward/away from the midline might be defective in PCNs treated with *Calm1*sh361 or *Calm1*sh427. Previous reports that showed that the action of midline guidance cues, such as netrin 1 or slit, is regulated by calcium signaling (Hong et al., 2000; Xu et al., 2004; Guan et al., 2007) are consistent with this interpretation.

Development (2015) 142, 375-384 doi:10.1242/dev.112680

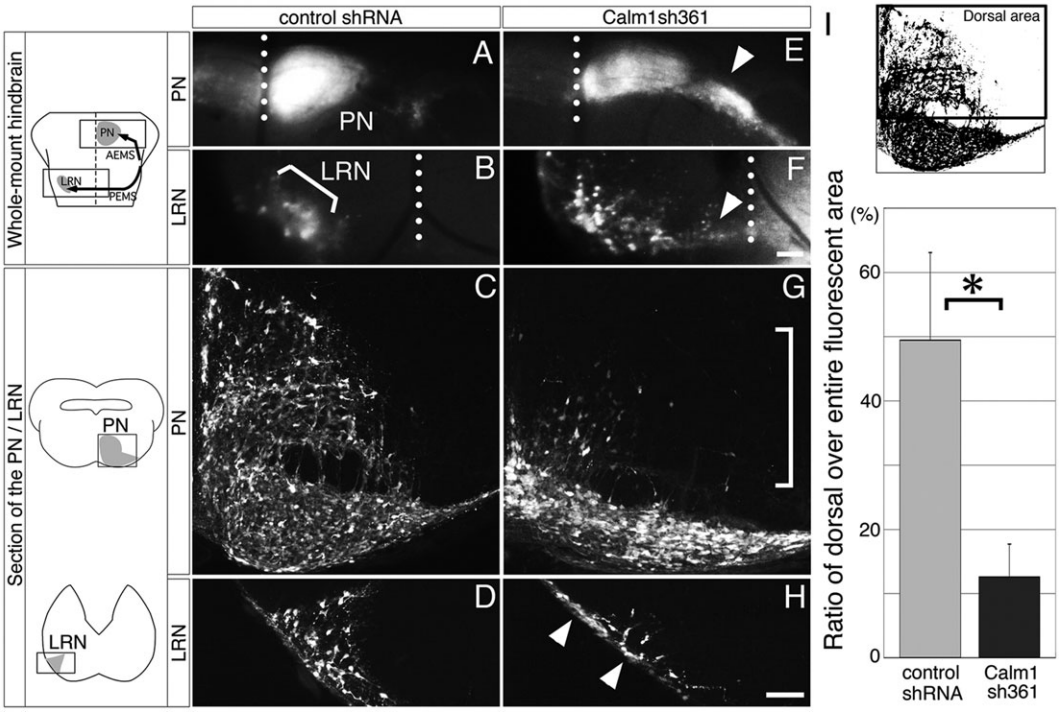

Fig. 8. Effects of *Calm1*sh361 on the migration of PCNs at E18.5. PCNs were co-transfected with GFP-expressing and control shRNA-expressing plasmids (A-D) or *Calm1*sh361-expressing plasmids (E-H) at E12.5 and examined at E18.5. (A,B,E,F) The distribution of GFP-labeled PCNs in whole-mount hindbrain, viewed ventrally, at the PN (A,E) and the LRN (B,F). (C,D,G,H) The distribution of GFP-labeled PCNs in transverse sections of the PN (C,G) and the LRN (D,H). Dotted lines indicate the midline. Arrowheads (E,F,H) indicate aberrantly positioned PCNs. The areas imaged are indicated to the left. Scale bar: 200 µm in A,B,E,F; 100 µm in C,D,G,H. (I) Quantification of dorsally located PN neurons. Shown is the ratio of the fluorescent dorsal area over the entire area of fluorescent PN neurons in the delineated region shown above (mean±s.d.). **P*<0.01, Mann–Whitney *U*-test; *n*=5 brains (15 sections) for control; *n*=5 brains (15 sections) for *Calm1*sh361.

Alternatively, the failure to reach the target region could be explained by defective neuronal motility, since Ca^{2+} signaling has been implicated in somal translocation. Ca^{2+} imaging and pharmacological perturbation studies have revealed a correlation between Ca^{2+} fluctuations in the soma and the rate of somal translocation in cerebellar granule cells (Komuro and Rakic, 1996, 1998; Kumada and Komuro, 2004). At the molecular level, nuclear translocation requires microtubule-based motors at the proximal region of the leading process and acto-myosin contraction at the trailing process (reviewed by Marín et al., 2006; Bellion et al., 2005; Martini and Valdeolmillos, 2010). Some proteins involved in this process, such as IQGAP1 and myosin light chain kinase, are regulated by CaM (Bagchi et al., 1992; Kholmanskikh et al., 2006; Marín et al., 2006). In accordance with these reports, we observed that *Calm1* transcripts are expressed at high levels at the proximal region of the leading process, and in the trailing process. Therefore, it is conceivable that nucleokinesis is affected in PCNs treated with *Calm1*sh361. It will be necessary to study the motility of these neurons to confirm this theory.

The absence of a clear nucleus structure at the target region suggests the possible involvement of *Calm1* in radial migration, although the defective neuronal motility discussed above might also have contributed to the failed radial migration. Radial migration is initiated by a turning or *de novo* formation of the leading process in the radial direction (Watanabe and Murakami, 2009). PCNs then radially migrate in close association with radial glial fibers (Kawauchi et al., 2006). We found that, with *Calm1*sh361 treatment, the leading population of PN neurons that had reached the midline at E15.5 rarely oriented along the radial glial fibers (Fig. 7D,J). The majority of PN neurons remained at the pial side of the prospective nucleus until E17.5, while the number of PN neurons that arrived gradually increased. Recently, it was shown that the radial migration of cortical neurons along the radial glia requires the gap junction subunit connexin 43 (Cx43; also known as Gja1), which is expressed at the contact points of migrating neurons and glial fibers and has a binding site for CaM (Elias et al., 2007; Zou et al., 2014). Therefore, the ability of PN neurons treated with *Calm1*sh361 to recognize radial glia should be investigated in future studies.

In summary, the present study has suggested a role of *Calm1* in several aspects of neuronal migration. It has been reported that *Calm1* is required for the migration of neuroblasts in the rostral migratory stream (Khodosevich et al., 2009). Neuroblasts originate in the subventricular zone of the lateral ventricles and migrate to the olfactory bulb, where they mature into granule and periglomerular cells. Silencing the expression of *Calm1* results in retarded migration and a decrease in the ratio of radial versus tangential migration in the target olfactory bulb (Khodosevich et al., 2009), similar to the defects observed in the present study. Together, these findings suggest that *Calm1* is essential for the migration of many neuronal types.

Relative contribution of the three CaM genes in PCN migration

The physiological significance of the existence of multiple CaM genes that each encode the exact same protein remains unknown. Since CaM has to interact with a diverse array of targets in a temporally and spatially regulated manner within a single cell, a plausible hypothesis is that each CaM transcript is differentially processed through post-transcriptional regulation and provides

Development (2015) 142, 375-384 doi:10.1242/dev.112680

distinct intracellular local CaM pools to ensure independent localization and size of the pools (Toutenhoofd and Strehler, 2000). This hypothesis postulates that all three CaM genes are expressed in the same cell and implies that they can have different cellular functions.

The simultaneous expression of multiple CaM genes in a cell has been deduced from their similar tissue expression profiles (Fig. 1) (Ikeshima et al., 1993; Solà et al., 1996; Palfi et al., 1999). In fact, the expression of all three CaM genes in a single cell type was shown previously in PC12 phechromocytoma and IMR-32 neuroblastoma cell lines (Zhang et al., 1993; Toutenhoofd and Strehler, 2002). The present study has, for the first time, revealed that a single neuron simultaneously expresses multiple CaM genes. This expression pattern raises the possibility that the three CaM genes are not used in a cell type-specific or temporally segregated manner, but are simultaneously used in the same cell, supporting the CaM local pool hypothesis discussed above.

Different cellular functions attributed to the three CaM genes have been deduced from their differential subcellular mRNA localizations. In hippocampal neurons, dendritic targeting of *Calm1* and *Calm3* but not *Calm2* transcripts was shown, suggesting their differential usage (Palfi et al., 1999, 2005). In our study, mRNAs of all three CaM genes were localized in the proximal region of the leading process. However, the transcripts rarely colocalized, raising the possibility that their processing is differentially regulated by functionally distinct RNA processing machinery, such as RNA granules or P-bodies (Krichevsky and Kosik, 2001; Kiebler and Bassell, 2006; Zeitelhofer et al., 2008). Our finding that the functional contribution of CaM gene family members in neuronal migration is not equal, but dominated by *Calm1*, supports this idea. However, to confirm this theory a more accurate evaluation of the amount of protein translated from each CaM gene is necessary in future studies.

In conclusion, the current study demonstrates that Ca^{2+}-CaM signaling is essential for neuronal migration. The involvement of CaM in transducing midline guidance signals and in somal translocation implied by this study is in accordance with previous reports suggesting that Ca^{2+} signaling regulates these events. Our study also suggested the involvement of CaM in the radial migration along radial glial fibers. Further studies on the dynamics of *Calm1*sh361-treated PCNs are needed to confirm these interpretations, and future work on the interaction with radial glia should shed light on the molecular mechanism that regulates radial migration.

MATERIALS AND METHODS

Animals

For all experiments, we used inbred ICR mouse strains obtained from Japan SLC (Hamamatsu, Japan). Noon of the day of vaginal plug detection was considered embryonic day (E) 0.5. For *exo utero* and *in utero* electroporation, pregnant mice were anesthetized by intraperitoneal injection of sodium pentobarbital (50 mg/kg body weight). All animal procedures were performed according to the guidelines of the Osaka University Animal Care Committee.

In situ hybridization

Complementary DNA sequences corresponding to the 3′UTR (500-700 nt in length) of each Calm family member were cloned into a pGEM-T Easy plasmid (Promega) using the following primers (5′-3′): Calm1Forward, CCCTCTGTCCACACACAAAG; Calm1Reverse, TTGATGGTGTGCTCAAGTCC; Calm2Forward, TTTATTTGCCTTTTCTTTGTTTG; Calm2Reverse, TGGATTTGAGGCAAGTTGTG; Calm3Forward, CCAAAAGATTTGTCCCAAGC; and Calm3Reverse, GCATGGGATGTTAGCACCAG. DIG-labeled antisense cRNA probes were transcribed using a linear template of the above plasmids and used to distinguish the three Calm genes.

ISH on 20 µm- or 30 µm-thick cryosections was performed as previously described (Kobayashi et al., 2013). ISH on cultured PCNs was performed as described (Kobayashi et al., 2005), with some minor modifications. Before hybridization, PCNs were acetylated in 0.25% acetic anhydride in 0.1 M triethanolamine and were refixed in 1% paraformaldehyde. Hybridization was performed at 55°C for 42 h. After the detection of bound cRNA probes, anti-MAP2 staining and nuclear staining with DAPI were performed.

Double FISH on cultured PCNs was carried out essentially as above, except that fluorescein-labeled cRNA probes were used along with DIG-labeled probes. The detection of each cRNA probe was carried out sequentially as follows. The culture was first reacted with anti-fluorescein-POD (Roche) and then FITC-tyramide (PerkinElmer). After inactivation of POD with 0.3% H_2O_2 for 30 min and extensive washes, the culture was reacted with anti-DIG-POD (Roche), followed by Cy3-tyramide (PerkinElmer), and the culture was then processed for nuclear staining with DAPI.

Immunohistochemistry

Primary antibodies used were: rabbit anti-nestin antibody (1:2000; rat 401, kind gift from Dr Arimatsu), rabbit anti-ssDNA polyclonal (1:100; IBL 18731), mouse anti-MAP2 monoclonal (1:200; Chemicon, MAB3418), rabbit anti-GFP polyclonal (1:500; MBL, M048-3), rat anti-GFP monoclonal (1:1000; Nacalai Tesque, clone GF090R) and chick anti-GFP polyclonal (1:1000; Abcam, ab13970). Secondary antibodies used were: Cy3-conjugated goat anti-rabbit IgG (1:200; Jackson ImmunoResearch, 111-165-144), Cy3-conjugated goat anti-mouse IgG (1:200; Jackson ImmunoResearch, 115-165-020), Alexa 488-conjugated goat anti-rabbit IgG (1:200; Invitrogen, A11008), Alexa 488-conjugated goat anti-rat IgG (1:200; Invitrogen, A11006) and Alexa 488-conjugated goat anti-chick IgG (1:200; Jackson ImmunoResearch, 103-545-155). For nuclear staining, cultured PCNs were reacted with 0.5 µg/ml DAPI solution. Mounting medium consists of 9.6% MOWIOL 4-88 (Calbiochem) containing 2.5% 1,4-diazobicyclo-(2,2,2)-octane (DABCO) (Sigma) to reduce fading.

Plasmid construction

The construction of shRNA-producing plasmids was carried out following the manufacturer's instructions (pSuper vector, OligoEngine). Briefly, a double-stranded DNA consisting of a sense target sequence followed by a hairpin and an antisense target sequence was ligated into the *Bgl*II/*Hin*dIII site of a pSUPER vector (OligoEngine). Target sequences for each Calm shRNA were (5′-3′): *Calm1*sh361, GAAGT-AGATGAAATGATCA; *Calm1*sh427, GTACA-GATGATGACTGCAA; *Calm2*sh414, CTACGA-AGAGTTTGTACAA; *Calm2*sh285, GGATG-GCAATGGCTATATT; *Calm3*sh384, GGCCGAC-ATTGATGGAGAT; and *Calm3*sh408, GGTC-AATTATGAAGAGTTT. Numbering of shRNAs refers to the nucleotide numbers in the CaM-coding sequence (the first nucleotide in the coding sequence was defined as +1).

Cell culture

COS7 cell culture, and the assessment of knockdown efficiency and specificity of shRNAs, were performed as previously described (Kobayashi et al., 2013). In brief, equal volumes of plasmid DNA solution [containing 1 µg/ml EYFP-Calm, 1 µg/ml mCherry and 8 µg/ml shRNA in OPTI-MEM (Life Technologies)] and Lipofectamine (Life Technologies) solution (20 µl/ml in OPTI-MEM) were mixed, and 50 µl DNA-Lipofectamine complex was added directly to 500 µl COS7 cell culture in a 24-well plate. After 24 h, transfection was terminated by replacing the culture medium with fresh medium, and cells were cultured for another 24 h and then fixed and processed for quantification. Fluorescence images were taken by confocal laser microscopy (TCS-SP2, Leica). Expression of the target EYFP-tagged CaM was measured as the ratio of total pixel intensity of EYFP to that of mCherry for each image. Knockdown efficiency was expressed as the ratio of EYFP-CaM expression (normalized by mCherry as above) in shRNA-treated cells to that in control cells.

Development (2015) 142, 375-384 doi:10.1242/dev.112680

To culture PCNs, the LRL of E12.5 hindbrain was excised and placed on 15-mm round coverslips pre-coated with poly-L-lysine solution (1 mg/ml). The explants were overlaid with 20 µl Matrigel (Matrigel Basement Membrane Matrix, BD) and cultured with DMEM/F12 supplemented with 10% FBS and 2% N2 supplement (Gibco). After 3 days *in vitro*, the culture was fixed and processed for ISH.

Real-time quantitative PCR

The LRL was electroporated with GFP-expressing plasmids at E12.5, and the prospective PN regions containing GFP-labeled PN neurons were dissected from E15.5 embryos. Tissues from six to ten embryos were pooled and dissociated by trypsinization and by pipetting through the narrow tip of a fire-polished Pasteur pipette. GFP-positive PCNs were then collected using a fluorescence-assisted cell sorter (FACSCalibur Flow Cytometry System, BD). About 500-5000 GFP-labeled PCNs were collected for each experimental condition. RNAs were extracted from these cells using the RNeasy Micro Kit (Qiagen) following the manufacturer's instructions and converted to cDNA using SuperScript III reverse transcriptase (Life Technologies). CaM mRNA content was quantified by real-time quantitative PCR with SYBR Green I on a LightCycler (Roche). To measure the absolute copy number of each CaM mRNA in a cDNA sample, standard curves were generated from quantifiable CaM cDNA cloned into plasmids. Normalization of cDNA content between samples was achieved by measuring internal control genes *Ppia* and *Actb*.

Electroporation

Exo utero electroporation and *in utero* electroporation were performed as previously described (Kawauchi et al., 2006; Kobayashi et al., 2013). In brief, plasmid solution (final concentration of 1 µg/µl pCAG-EGFP, 1.5 µg/µl pSUPER-shRNA plasmid) containing 0.01% Fast Green was injected into the fourth ventricle of E12.5 mouse embryos, and DNA was electroporated into the LRL. The embryos were then allowed to continue normal development *in utero*.

For the sparse labeling, we co-introduced pCALNL-EGFP and pCAG-Cre. In this system, the expression of EGFP is prevented by an upstream neomycin resistance gene flanked by *loxP* sequences. EGFP expression is achieved by excision of the neomycin sequence by Cre recombinase (Kanegae et al., 1995). We combined 1 ng/µl pCAG-Cre and 1 µg/µl pCALNL-EGFP for appropriate labeling density.

Image analysis

Fluorescence images were taken with a digital camera (AxioCaM, Zeiss) and analyzed with Metamorph software (Universal Imaging). To quantify the dorsoventral distribution of PCNs in the E17.5 PN, a 667 µm×667 µm square and its dorsal two-thirds were delineated. Total pixel area showing EGFP fluorescence above threshold was measured for each square, and the ratio of the fluorescent area in the dorsal two-thirds to that of the entire square was calculated. For quantification in the E18.5 PN, a 800 µm×800 µm square and its dorsal two-thirds were used. To quantify the ratio of radially migrating PN neurons at E15.5, fluorescent cells within 435 µm of the midline were analyzed. The percentage of radially migrating neuronal area among the entire fluorescent area was calculated. To quantify PN neurons in the migratory pathway, the ratio of the fluorescent cell area located farther than 640 µm from the midline to that of the entire section was calculated. Three to four sections 80-90 µm apart were chosen and analyzed for each brain. Data were analyzed statistically with the Mann–Whitney *U*-test for comparisons between the control and each shRNA-treated group. $P<0.01$ was considered significant.

Acknowledgements

We thank Dr Tetsuichiro Saito for the *Mbh2* plasmid; Keisuke Takeda, Yuma Sato, Yuto Hashimoto, Shota Ogata, Hideharu Hayashi, Masashi Motomura for technical assistance; and Peter Karagiannis for editing the manuscript.

Competing interests

The authors declare no competing financial interests.

Author contributions

H.K. and F.M. designed the study. H.K., S.S., A.N. and K.I. performed the experiments. H.K. and A.N. performed the expression analysis. H.K., S.S. and K.I. performed functional assays. D.K. established the foundation of the experimental system. H.K. and F.M. wrote the paper.

Funding

This work was supported by Grants-in-Aid from MEXT, Japan [17023028].

References

Altman, J. and Bayer, S. A. (1987a). Development of the precerebellar nuclei in the rat: III. The posterior precerebellar extramural migratory stream and the lateral reticular and external cuneate nuclei. *J. Comp. Neurol.* **257**, 513-528.

Altman, J. and Bayer, S. A. (1987b). Development of the precerebellar nuclei in the rat: IV. The anterior precerebellar extramural migratory stream and the nucleus reticularis tegmenti pontis and the basal pontine gray. *J. Comp. Neurol.* **257**, 529-552.

Altman, J. and Bayer, S. A. (1997). *Development of the cerebellar system. In Relation to Its Evolution, Structure, and Functions*, pp. 266-321. Boca Raton: CRC Press.

Ayala, R., Shu, T. and Tsai, L.-H. (2007). Trekking across the brain: the journey of neuronal migration. *Cell* **128**, 29-43.

Bagchi, I. C., Huang, Q. H. and Means, A. R. (1992). Identification of amino acids essential for calmodulin binding and activation of smooth muscle myosin light chain kinase. *J. Biol. Chem.* **267**, 3024-3029.

Bellion, A., Baudoin, J.-P. Alvarez, C., Bornens, M. and Métin, C. (2005). Nucleokinesis in tangentially migrating neurons comprises two alternating phases: forward migration of the golgi/centrosome associated with centrosome splitting and myosin contraction at the rear. *J. Neurosci.* **25**, 5691-5699.

Berggård, T., Arrigoni, G., Olsson, O., Fex, M., Linse, S. and James, P. (2006). 140 mouse brain proteins identified by Ca^{2+}-calmodulin affinity chromatography and tandem mass spectrometry. *J. Proteome Res.* **5**, 669-687.

Bulfone, A., Menguzzato, E., Broccoli, V., Marchitiello, A., Gattuso, C., Mariani, M., Consalez, G. G., Martinez, S., Ballabio, A. and Banfi, S. (2000). *Barhl1*, a gene belonging to a new subfamily of mammalian homeobox genes, is expressed in migrating neurons of the CNS. *Hum. Mol. Genet.* **9**, 1443-1452.

Elias, L. A. B., Wang, D. D. and Kriegstein, A. R. (2007). Gap junction adhesion is necessary for radial migration in the neocortex. *Nature* **448**, 901-907.

Friedberg, F. and Rhoads, A. R. (2001). Evolutionary aspects of calmodulin. *IUBMB Life* **51**, 215-221.

Guan, C.-b., Xu, H.-t., Jin, M., Yuan, X.-b. and Poo, M.-m. (2007). Long-range Ca^{2+} signaling from growth cone to soma mediates reversal of neuronal migration induced by Slit-2. *Cell* **129**, 385-395.

Hatten, M. E. (2002). New directions in neuronal migration. *Science* **297**, 1660-1663.

Hong, K., Nishiyama, M., Henley, J., Tessier-Lavigne, M. and Poo, M.-m. (2000). Calcium signalling in the guidance of nerve growth by netrin-1. *Nature* **403**, 93-98.

Ikeshima, H., Yuasa, S., Matsuo, K., Kawamura, K., Hata, J. and Takano, T. (1993). Expression of three nonallelic genes coding calmodulin exhibits similar localization on the central nervous system of adult rats. *J. Neurosci. Res.* **36**, 111-119.

Ikura, M. and Ames, J. B. (2006). Genetic polymorphism and protein conformational plasticity in the calmodulin superfamily: two ways to promote multifunctionality. *Proc. Natl. Acad. Sci. USA* **103**, 1159-1164.

Kanegae, Y., Lee, G., Sato, Y., Tanaka, M., Nakal, M., Sakaki, T., Sugano, S. and Saito, I. (1995). Efficient gene activation in mammalian cells by using recombinant adenovirus expressing site-specific Cre recombinase. *Nucleic Acids Res.* **23**, 3816-3821.

Kawauchi, D., Taniguchi, H., Watanabe, H., Saito, T. and Murakami, F. (2006). Direct visualization of nucleogenesis by precerebellar neurons: involvement of ventricle-directed, radial fibre-associated migration. *Development* **133**, 1113-1123.

Khodosevich, K., Seeburg, P. H. and Monyer, H. (2009). Major signaling pathways in migrating neuroblasts. *Front. Mol. Neurosci.* **2**, 7.

Kholmanskikh, S. S., Koeller, H. B., Wynshaw-Boris, A., Gomez, T., Letourneau, P. C. and Ross, M. E. (2006). Calcium-dependent interaction of Lis1 with IQGAP1 and Cdc42 promotes neuronal motility. *Nat. Neurosci.* **9**, 50-57.

Kiebler, M. A. and Bassell, G. J. (2006). Neuronal RNA granules: movers and makers. *Neuron* **51**, 685-690.

Kobayashi, H., Yamamoto, S., Maruo, T. and Murakami, F. (2005). Identification of a *cis*-acting element required for dendritic targeting of activity-regulated cytoskeleton-associated protein mRNA. *Eur. J. Neurosci.* **22**, 2977-2984.

Kobayashi, H., Kawauchi, D., Hashimoto, Y., Ogata, T. and Murakami, F. (2013). The control of precerebellar neuron migration by RNA-binding protein Csde1. *Neuroscience* **253**, 292-303.

Komuro, H. and Rakic, P. (1996). Intracellular Ca^{2+} fluctuations modulate the rate of neuronal migration. *Neuron* **17**, 275-285.

Komuro, H. and Rakic, P. (1998). Orchestration of neuronal migration by activity of ion channels, neurotransmitter receptors, and intracellular Ca^{2+} fluctuations. *J. Neurobiol.* **37**, 110-130.

Development (2015) 142, 375-384 doi:10.1242/dev.112680

Krichevsky, A. M. and Kosik, K. S. (2001). Neuronal RNA granules: a link between RNA localization and stimulation-dependent translation. *Neuron* **32**, 683-696.
Kumada, T. and Komuro, H. (2004). Completion of neuronal migration regulated by loss of Ca^{2+} transients. *Proc. Natl. Acad. Sci. USA* **101**, 8479-8484.
Li, S., Qiu, F., Xu, A., Price, S. M. and Xiang, M. (2004). *Barhl1* regulates migration and survival of cerebellar granule cells by controlling expression of the neurotrophin-3 gene. *J. Neurosci.* **24**, 3104-3114.
Marín, O., Valdeolmillos, M. and Moya, F. (2006). Neurons in motion: same principles for different shapes? *Trends Neurosci.* **29**, 655-661.
Marín, O., Valiente, M., Ge, X. and Tsai, L.-H. (2012). Guiding neuronal cell migrations. *Cold Spring Harb. Perspect. Biol.* **2**, a001834.
Martini, F. J. and Valdeolmillos, M. (2010). Actomyosin contraction at the cell rear drives nuclear translocation in migrating cortical interneurons. *J. Neurosci.* **30**, 8660-8670.
Okada, T., Keino-Masu, K. and Masu, M. (2007). Migration and nucleogenesis of mouse precerebellar neurons visualized by in utero electroporation of a green fluorescent protein gene. *Neurosci. Res.* **57**, 40-49.
Palfi, A., Vizi, S. and Gulya, K. (1999). Differential distribution and intracellular targeting of mRNAs corresponding to the three calmodulin genes in rat brain: a quantitative in situ hybridization study. *J. Histochem. Cytochem.* **47**, 583-600.
Palfi, A., Kortvely, E., Fekete, E., Kovacs, B., Varszegi, S. and Gulya, K. (2002). Differential calmodulin gene expression in the rodent brain. *Life Sci.* **70**, 2829-2855.
Palfi, A., Kortvely, E., Fekete, E. and Gulya, K. (2005). Multiple calmodulin mRNAs are selectively transported to functionally different neuronal and glial compartments in the rat hippocampus. an electron microscopic in situ hybridization study. *Life Sci.* **77**, 1405-1415.
Shinohara, M., Zhu, Y. and Murakami, F. (2013). Four-dimensional analysis of nucleogenesis of the pontine nucleus in the hindbrain. *J. Comp. Neurol.* **521**, 3340-3357.
Solà, C., Tusell, J. M. and Serratosa, J. (1996). Comparative study of the pattern of expression of calmodulin messenger RNAs in the mouse brain. *Neuroscience* **75**, 245-256.
Taber Pierce, E. (1966). Histogenesis of the nuclei griseum pontis, corporis pontobulbaris and reticularis tegmenti pontis (Bechterew) in the mouse. An autoradiographic study. *J. Comp. Neurol.* **126**, 219-239.
Taber Pierce, E. (1973). Time of origin of neurons in the brain stem of the mouse. *Prog. Brain Res.* **40**, 53-65.
Toutenhoofd, S. L. and Strehler, E. E. (2000). The calmodulin multigene family as a unique case of genetic redundancy: multiple levels of regulation to provide spatial and temporal control of calmodulin pools? *Cell Calcium* **28**, 83-96.
Toutenhoofd, S. L. and Strehler, E. E. (2002). Regulation of calmodulin mRNAs in differentiating human IMR-32 neuroblastoma cells. *Biochim. Biophys. Acta* **1600**, 95-104.
Watanabe, H. and Murakami, F. (2009). Real time analysis of pontine neurons during initial stages of nucleogenesis. *Neurosci. Res.* **64**, 20-29.
Xu, H.-t., Yuan, X.-b., Guan, C.-b., Duan, S., Wu, C.-p. and Feng, L. (2004). Calcium signaling in chemorepellant Slit2-dependent regulation of neuronal migration. *Proc. Natl. Acad. Sci. USA* **101**, 4296-4301.
Zeitelhofer, M., Karra, D., Macchi, P., Tolino, M., Thomas, S., Schwarz, M., Kiebler, M. and Dahm, R. (2008). Dynamic interaction between P-bodies and transport ribonucleoprotein particles in dendrites of mature hippocampal neurons. *J. Neurosci.* **28**, 7555-7562.
Zhang, S.-P., Natsukari, N., Bai, G., Nichols, R. A. and Weiss, B. (1993). Localization of the multiple calmodulin messenger RNAs in differentiated PC12 cells. *Neuroscience* **55**, 571-582.
Zheng, J. Q. and Poo, M.-m. (2007). Calcium signaling in neuronal motility. *Annu. Rev. Cell Dev. Biol.* **23**, 375-404.
Zou, J., Salarian, M., Chen, Y., Veenstra, R., Louis, C. F. and Yang, J. J. (2014). Gap junction regulation by calmodulin. *FEBS Lett.* **588**, 1430-1438.